ACS OMEGA

Open Access

http://pubs.acs.org/journal/acsodf

Article

Manganese Carbonate/Laser-Induced Graphene Composite for Glucose Sensing

Amit K. Thakur,[‖] Prakash Sengodu,[‖] Arvind H. Jadhav, and Mahdi Malmali*

Cite This: *ACS Omega* 2024, 9, 7869−7880

Read Online

ACCESS | Metrics & More | Article Recommendations | Supporting Information

ABSTRACT: Laser-induced graphene (LIG) has received great interest as a potential candidate for electronic and sensing applications. In the present study, we report the enhanced performance of a manganese carbonate-decorated LIG ($MnCO_3$/LIG) composite electrode material employed for electrochemical glucose detection. Initially, the porous LIG was fabricated by directly lasing poly(ether sulfone) membrane substrate. Then, the $MnCO_3$/LIG composite was synthesized via a hydrothermal method. Later, $MnCO_3$/LIG was immobilized onto a glassy carbon electrode surface and employed for glucose detection. The structure of the $MnCO_3$/LIG composite was carefully characterized. The influence of the $MnCO_3$/LIG composite on the performance of the electrode was investigated using cyclic voltammetry curves. The $MnCO_3$/LIG composite exhibited an excellent sensitivity of 2731.2 μA mM^{-1} cm^{-2}, and a limit of detection of 2.2 μM was obtained for the detection of glucose. Overall, the performance of the $MnCO_3$/LIG composite was found to be superior to that of most of the $MnCO_3$-based composites.

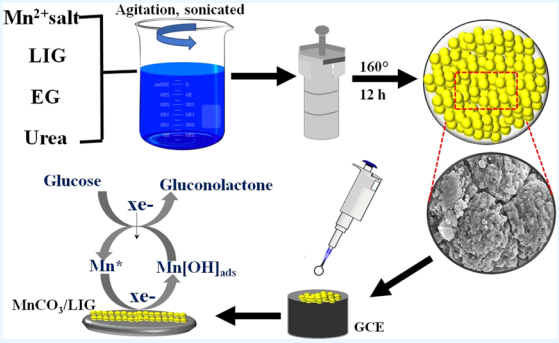

INTRODUCTION

Diabetes is a metabolic disorder and a dangerous disease that affects millions of people worldwide.[1] According to the World Health Organization and the International Diabetes Federation studies, ∼422 million people are diabetic, and this will increase to 642 million by 2030. Diabetes causes long-term complications in the human body, such as disturbing the nerves, kidneys, blood vessels, eyes, and skin.[2] Treatment for diabetes has become a far more sophisticated science, and the demand for self-testing of glucose levels in the blood has increased; hence, more compact sensors with higher accuracy are of significant commercial interest. The design and development of reliable and precise sensors for the detection of glucose at very low levels in the presence of interference are highly required. Glucose oxidase (GOx)-based enzymatic glucose biosensors have been widely used in the past decades due to their high selectivity and reliability.[3] For example, platinum nanoparticles and GOx were in situ synthesized and immobilized on the surface of the eggshell membrane and were successfully demonstrated for glucose detection.[4] Enzymatic glucose sensors based on chitosan electrodes were also reported recently.[5] The major obstacle with GOx enzymes is the fact that they suffer from the degradation of enzyme activity, as well as the performance variation in the environment.[6] Hence, enzyme-free glucose sensors have received more attention for the upcoming generation of sensors.[2,7] Various materials have been exploited for enzyme-free glucose biosensors, such as metal nanoparticles,[8−10] carbon-supported composites,[11−13] alloys,[14,15] and carbon nanotubes.[16,17] Proposed sensors, however, also have some shortcomings, such as low sensitivity, poor selectivity, cost, and chloride poisoning, which limit the widespread application of such sensors. Therefore, there is an imperative need to develop cost-effective, highly sensitive, and selective electrodes for enzyme-free glucose sensors.

For the fabrication of high-performance biosensors, the usage of graphene is a rational choice due to its unique properties such as tunable electronic properties, including charge concentration, mobility and density, band gap, and electron transfer rate, which have enabled its application in a variety of electrochemical biosensors.[18] Moreover, the high surface area, large potential window, unique flexibility and robustness, and lower charge transfer resistance properties of graphene make it an ideal material for electrodes. Graphene was first used in polyethylenimine-functionalized ionic liquid nanocomposite-modified electrodes in glucose sensors.[19] In another study, a hybrid nanocomposite of graphene−chitosan was used to modify the glassy carbon electrode (GCE). The prepared glucose biosensors displayed excellent sensitivity (37.93 μA mM^{-1} cm^{-2}) and long-term durability.[20] It is

Received: October 2, 2023
Revised: December 22, 2023
Accepted: January 4, 2024
Published: February 5, 2024

reported that the chemically reduced graphene oxide (GP) showed improved amperometric signals for sensing glucose, linear sensing in the range of 0.01−10 mM, limit of detection (LOD) of 2 μM, and sensitivity of 20.21 μA mM^{-1} cm^{-2}.[21] It is also reported that nitrogen-doped graphene improved the electrochemical performance of enzymatic glucose sensors.[22] Gold nanoparticles (AuNPs)-decorated thionine functionalized GO, in which AuNPs were densely anchored over GO sheets with the aid of thionine, displayed improved glucose sensing (LOD of 0.05 μM). This enhanced glucose sensing was attributed to the synergies in the performance of the three components.[23] Au−GO was reported as an enzyme-free glucose sensor for a wide range of concentration (i.e., 0.05−40 mM) with linearity outputs in the range of 1−10 mM.[24] Pt nanoclusters/graphene nanocomposite showed a sensitivity of 1.21 μA mM^{-1} cm^{-2} with a fast response (i.e., 3 s) for glucose sensing in neutral media.[25] Pt−Au/MnO_2 deposited on graphene sheet was demonstrated for significantly improved glucose sensing performance with a concentration range of 0.1−30.0 mM, sensitivity of 58.54 μA mM^{-1} cm^{-2}, low LOD of 0.02 mM, satisfactory selectivity, outstanding reproducibility and stability, and mechanical stress tolerability.[26] In another report, Mn_3O_4 NPs were decorated on N-doped graphene (Mn_3O_4NPs/N-GR). Then, Mn_3O_4NPs/N-GR was filled into a glassy tube to prepare the carbon paste electrode, which displayed a sensitivity of 0.1011 μA μM^{-1}.[27] Mn_3O_4 NPs decorated on N-doped rGO were also reported to be an excellent enzyme-free glucose sensor with reasonable sensitivity (i.e., 0.026 μA μM^{-1}) and good selectivity.[28] Graphene aerogel@AuNPs/AuNPs were designed for enzyme-free glucose sensor and exhibited excellent LOD of 3 μM, with a linear range of 0.01−16 mM. The improved performance of the sensor was attributed to the largely enhanced electron transfer, mass transport, and catalytic activity of graphene and the AuNPs.[29]

Tour and co-workers reported that polymeric substrates such as polyimide (PI) could be photothermally converted into 3D porous graphene, also known as laser-induced graphene (LIG).[30] Later, many studies focused on the formation of LIG on various carbonaceous substrates, including poly(ether sulfone) (PES), polysulfone (PSF), polyphenylsulfone (PPSU), and naturally available materials.[31−33] Since its discovery, LIG has emerged as an important material for diverse applications because of its reagent-free preparation and potentially straightforward route for scale-up.[34] Its high electrical conductivity, porosity, flexibility, and hydrophilicity/hydrophobicity have been extensively exploited in many applications, such as sensors,[35,36] electronics,[32] flexible heaters,[37] water treatment,[38] and adsorption.[39,40]

To date, there are very few reports on LIG-based glucose sensors. Zhu et al. prepared glucose sensors by electroless plating of the gold and nickel on LIG electrodes and evaluated their performance for nonenzymatic glucose sensing.[41] In their study, they used PI-derived LIG, different precursors of Pd and Au, and Nafion resin to fabricate the working electrode. These materials are known to be expensive and rare, and the synthesis route requires extra processing steps and resources.[41] Settu et al. reported a chitosan-GOx-modified LIG electrode for glucose detection, which showed poor sensitivity (43.15 μA mM^{-1} cm^{-2})[42]; hence, it was not found to be suitable for real-time glucose sensing. In a different study, a composite of Co/CuNPs in LIG electrode was evaluated for nonenzymatic glucose sensors.[43,44] Despite a few recent studies on LIG-based glucose sensors, there is still a need to further improve the sensitivity of LIG composites that can provide better performance.

Numerous studies on manganese oxide-based sensors have been reported for nonenzymatic glucose detection. Flexible and freestanding glucose biosensor based on Mn_3O_4 grown on three-dimensional graphene foam (Mn_3O_4/3DGF) composite was reported.[45] Mn_3O_4 nanoparticles grown on nitrogen-doped graphene (NPs/N-GR) electrode provided a broader detection range of 2.5−529.5 μM for glucose sensor.[46] GC electrodes modified with bimetallic CoMn-based nanoparticles with hierarchical carbon (CoMnO@HC) displayed reasonable electrocatalytic activity for glucose in the range of 50−900 μM and 1.9−6.9 mM, with a sensitivity of 233.8 μA mM^{-1} cm^{-2}.[47] MnO_2 on multiwalled carbon nanotubes (MnO_2/MWNTs and Cu/MnO_2/MWCNTs) electrodes also displayed good sensitivity with resistance toward poisoning by chloride ions.[48,49] Multicomponent Nafion/Mn−Ni-oxide nanocomposite and nanosheets of $NiMn_2O_4$ on reduced graphene oxide ($NiMn_2O_4$NSs@rGO) were also demonstrated for nonenzymatic glucose sensors.[50,51] A glucose sensor based on α-MnO_2/Co_3O_4 composite electrode was also studied and demonstrated by Sinha et al.[52] Above-mentioned manganese oxide-based sensors have withstanding issues with respect to sensitivity and practical applications. In order to develop innovative nonenzymatic glucose sensors, manganese carbonate ($MnCO_3$) is being considered emerging candidate materials. The major obstacle to developing $MnCO_3$-based electrodes for electrochemical applications is its poor electronic conductivity.[53] To resolve this issue, $MnCO_3$ was directly grown on a nickel substrate to attain reasonable electrical conductivity and increase the contact area between the electrode material and electrolyte. $MnCO_3$/Ni foil electrode showed a glucose sensing potential of 0.55 V with a linear range of 0.001−0.5 mM and a sensitivity of 1254.4 μA mM^{-1} cm^{-2}.[54] Nonetheless, sensors made with this approach did not meet all of the required ideal sensing criteria, such as lower linear sensing ranges and threshold sensitivity. Further, the electrochemical behavior of bare $MnCO_3$ or nickel foil electrodes for glucose detection was not studied individually because glucose has shown an anodic response in basic solution at nickel electrodes. The catalytic NiOOH species is reduced to $Ni(OH)_2$ in the glucose oxidation mechanism through hydrogen abstraction of the C-1 hydrogen atom intermediate. Dehydrogenated radical is then oxidized to gluconolactone, which is finally converted to gluconic acid by hydrolysis.[55,56]

In this work, LIG was prepared by laser irradiation on a poly(ether sulfone) porous substrate. Then, $MnCO_3$/LIG composite was synthesized, characterized, and further used to fabricate an enzyme-free biosensor electrode for glucose detection in an alkaline medium. Cyclic voltammetry (CV) tests of LIG, bare $MnCO_3$, and $MnCO_3$/LIG composite-modified GC electrodes were performed with and without glucose. The effect of glucose concentration and scan rates on the $MnCO_3$/LIG composite-modified GC electrode performance was already studied. The amperometric response of the electrodes was also monitored and compared. Similarly, the effect of interference was studied with a $MnCO_3$/LIG composite-modified GC electrode, and its stability was assessed for 30 days.

https://doi.org/10.1021/acsomega.3c07642
ACS Omega 2024, 9, 7869−7880

EXPERIMENTAL SECTION

Materials. Poly(ether sulfone) (PES Veradel 3000P $M_w \sim$ 65,000 g mol^{-1}) was supplied by Solvay (GA, USA). Glucose, GOx, manganese acetate tetrahydrate (≥99%), and *N*-methyl-2-pyrrolidone (NMP) were purchased from Fisher Scientific (Pittsburgh, PA). Urea, sodium chloride (NaCl), and potassium chloride (KCl) were purchased from SD Fine Chemicals, India. Deionized (DI) water was used in all experiments. All other chemicals/reagents were used as received.

Fabrication of PES Porous Substrates. PES porous substrates were prepared by the nonsolvent-induced phase separation (NIPS), as follows. First, the PES powder was dried at 80 °C in a convection oven. Then, 20 g of dried PES powder was slowly added to 80 g of NMP solution at room temperature with vigorous stirring followed by heating at 60 °C for 6 h and further stirring at room temperature for 24 h. The bubble-free homogeneous PES solution was cast evenly on a clean glass plate using a Gardco casting knife film applicator, assisted with a Gardco automatic drawdown machine II (0.09 m per second speed and 0.09 m stroke length) with a casting thickness of 600 μm. The film was shortly exposed to the ambient air followed by immersion precipitation in a nonsolvent coagulation bath (DI water). After 0.5 h, the porous substrate was removed from the coagulation bath and placed in fresh DI water for 24 h to complete the phase inversion process and remove any residual solvent. Finally, the porous substrate was dried in a convection oven at 50 °C for 48 h.

Laser Irradiation of PES Porous Substrates. Laser irradiation of PES porous substrates was performed with a computer-controlled CO_2 laser system (Universal Laser System VLS 3.6, 40 W, wavelength 10.6 μm). The laser power was set to 8 W; the writing speed was 25.4 cm/s, and the image density was fixed at 1000 PPI (points per inch) in a raster mode under ambient conditions with air assist. The LIG layer was then scraped off from the PES substrate with a thin flat-end spatula and sonicated with an ultrasonic cleaner for 1 h. Then, the LIG powder was dried and stored for further use.

Preparation of $MnCO_3$ and $MnCO_3$/LIG Composite. Figure 1 illustrates the synthesis route of the $MnCO_3$/LIG composite material for glucose sensing. In the first step, the PES substrate was lased with a CO_2 infrared laser, leading to the formation of a carbon-rich microporous conductive graphene layer. This was followed by scraping and mixing with $MnCO_3$ to make the composite material. 0.75 g of manganese acetate tetrahydrate and 1.50 g of urea were dissolved in 60 mL of ethylene glycol with vigorous stirring for 30 min. The solution was transferred to autoclaves and kept at 160 °C for 12 h to synthesize $MnCO_3$. For the preparation of $MnCO_3$/LIG composites, 0.75 g of manganese acetate tetrahydrate, 0.06 g of LIG, and 1.50 g of urea were dispersed in 60 mL of ethylene glycol with continuous agitation and ultrasonicated for 20 min. The solution was later transferred to an autoclave and maintained at 160 °C for 12 h. The obtained samples were centrifuged and then washed with ethanol−water solution three times. The final product was dried at 100 °C for 12 h.

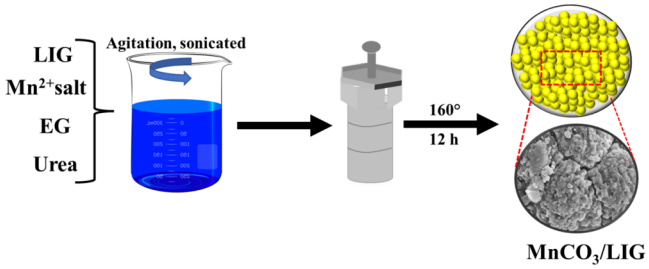

Figure 1. Preparation of LIG and $MnCO_3$/LIG composites and their fabrication.

Electrochemical Sensing. $MnCO_3$ or $MnCO_3$/LIG composite (10 mg) was mixed in 1 mL of DI water under sonication to form the inks. Approximately 3 μL of each ink was dropped onto a clean glassy carbon (GC) electrode (3 mm diameter) and dried at room temperature to form the modified GCE. Modified GCE was then transferred to the one-compartment electrochemical cell connected with Pt wire as a counter electrode and saturated calomel electrode as a reference electrode. All electrochemical experiments were performed using an electrochemical analyzer (CH Instruments, Model 680 Amp).

Characterizations. Scanning electron microscopy (SEM) images were obtained from a field emission scanning electron microscope (FE-SEM-JEOL Model-JSM7, Japan), equipped with an energy-dispersive spectrometer. Before the analysis, a thin layer of a gold and palladium alloy was evenly coated on the sample. High-resolution transmission electron microscopy (HR-TEM) images were taken by using a JEOL JEM-200CX operating at 200 kV. The powder X-ray diffraction (XRD) patterns were recorded on an X-ray diffractometer (XRD Rigaku, Japan). Raman spectra were collected using a Bruker Optics Senterra dispersive Raman microscope spectrometer with a 532 nm laser excitation. X-ray photoelectron spectroscopy (XPS) spectra of the composite were recorded on a PerkinElmer, PHI1257 (USA), with Al Kα source and excitation energy of 1486.7 eV; the binding energy was calibrated using C 1s at 284.5 eV. Fourier transform infrared (FTIR) spectroscopy was performed with a Spectrum Two (PerkinElmer, USA), equipped with an attenuated total reflection cell using the KBr pellet method. The porous structures of the materials were determined using a nitrogen adsorption isotherm obtained from the BELSORP MAX instrument II (Japan) surface analyzer. The materials were degassed at 200 °C for 2 h under a high vacuum before the measurement.

RESULTS AND DISCUSSION

As displayed in Figure 2a, XRD diffractogram of LIG powder scraped from the porous substrate shows a strong peak at ∼25.9°, corresponding to the interlayer spacing (∼0.34 nm) between (002) planes and a smaller peak centered at ∼42.8° associated with (100) reflection in the graphitic materials.[39,57] The XRD patterns of $MnCO_3$ and $MnCO_3$/LIG (Figure 2a) exhibit calcite-type rhombohedral structure and matched well with JCPDS No 86−0172.[58] Multiple sharp peaks were found at 2θ = 24.3, 31.5, 37.7, 41.6, 45.5, 50.0, 51.9, 60.4, 64.1, and 68.1°, which corresponded to the (012), (104), (110), (113), (202), (024), (116), (122), (214), and (300) planes of $MnCO_3$, respectively.[59] All of these peaks are retained in the $MnCO_3$/LIG composite, confirming the successful formation of the composite. Raman spectrum of LIG displayed in Figure 2b indicates that LIG has characteristic peaks for graphene: the D peak at ∼1346 cm^{-1} originating from defect and bending, the G peak at ∼1577 cm^{-1} confirming graphitization, and the

https://doi.org/10.1021/acsomega.3c07642
ACS Omega 2024, 9, 7869−7880

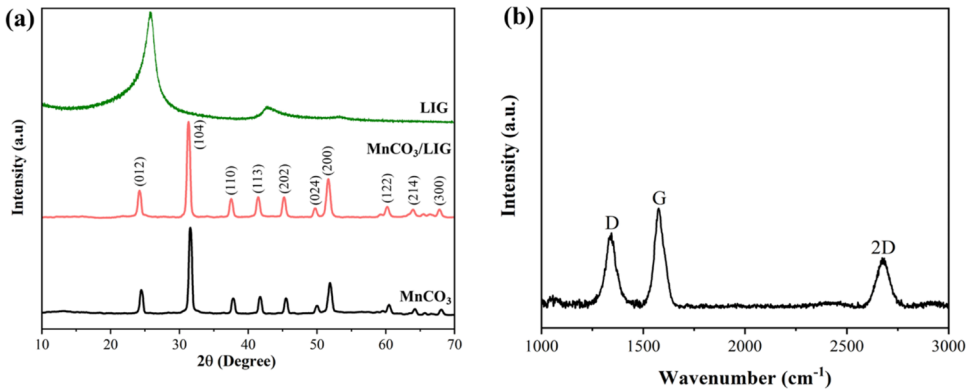

Figure 2. (a) XRD analysis of LIG, $MnCO_3$, and $MnCO_3$/LIG composite. (b) Raman spectra of LIG.

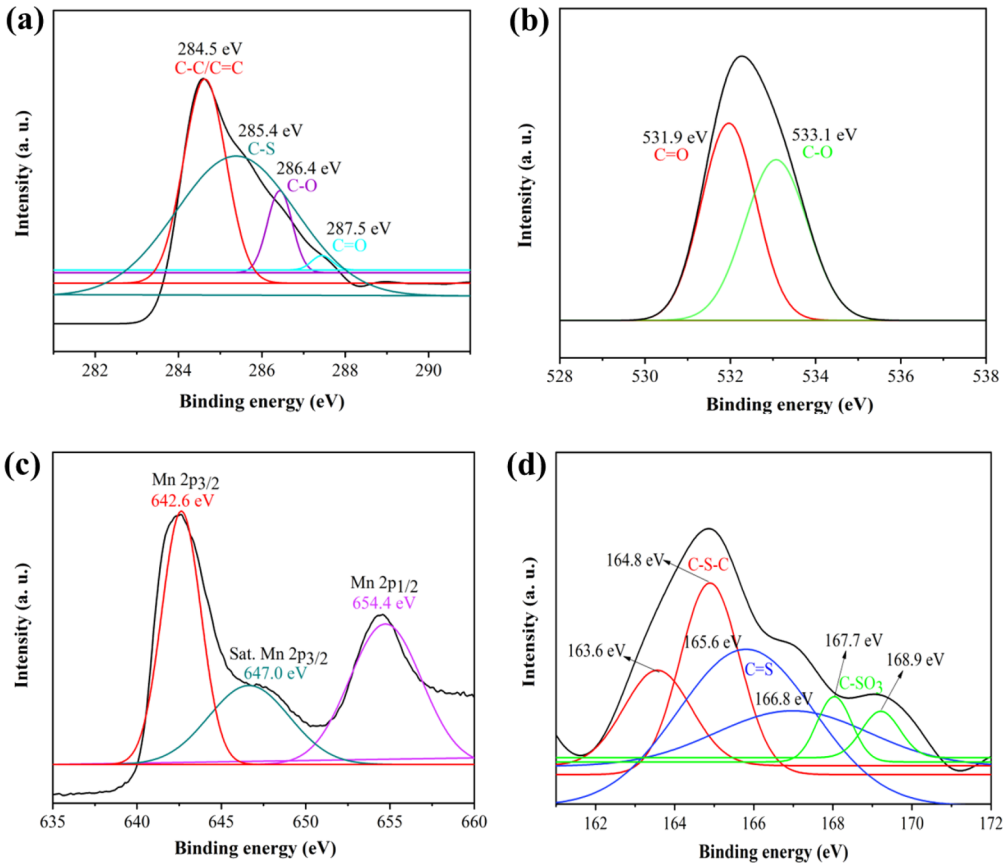

Figure 3. High-resolution XPS. (a) C 1s, (b) O 1s, (c) Mn 2p, and (d) S 2p for the $MnCO_3$/LIG composite.

2D peak at ~2690 cm^{-1} arising from multilayer graphene.[60,61] Samples were then characterized using XPS to study the atomic structure of the LIG and the $MnCO_3$/LIG composite. As shown in Figure S1a (Supporting Information), carbon, oxygen, and sulfur were observed in LIG, while manganese was seen in the LIG composite structure.

The high-resolution C 1s spectrum of LIG is shown in Figure S1b, which clearly indicates graphene formation. The functional groups and composing structure gave peaks centered at 284.5 (C═C/C−C), 285.3 (C−S), 286.3 (C−−O), 287.4 (C═O), and 288.6 eV (O−C═O).[62,63] The XPS C 1s spectrum of $MnCO_3$/LIG displayed in Figure 3a can be deconvoluted into four peaks corresponding to C−C/C═O (284.5 eV), C−S (285.4 eV), C−O (286.4), and C=O (287.5. eV).[39] The O 1s spectrum of composite demonstrates (Figure 3b) the existence of C═O and C−O functional groups at 531.9 and 533.1 eV.[39] In Figure 3c, two main peaks at 642.6 and 654.4 eV can be observed, which are characteristic peaks of $2p_{3/2}$ and $2p_{1/2}$ in Mn.[64] In addition, there is an additional peak fitted at 647.0 eV corresponding to the satellite peak of Mn $2p_{3/2}$ (indicated as "Sat.").[64] The S 2p peaks of the XPS spectra of the composite shown in Figure 3d can be deconvoluted into three species: C−S−C, C═S, and C−SO_3. The first two peaks at 163.6 and 164.8 eV correspond to the S $2p_{3/2}$ and S $2p_{1/2}$ of C−S−C bonded LIG,[39,65] whereas peaks at 165.6, 166.8, 167.7, and 168.8 eV attributed to the C═S and C−SO_3.[39,65]

The surface morphology of $MnCO_3$ and $MnCO_3$/LIG was studied by SEM, and low- and high-magnification images are provided in Figure 4. Figure 4a,b shows that $MnCO_3$ has

https://doi.org/10.1021/acsomega.3c07642
ACS Omega 2024, 9, 7869−7880

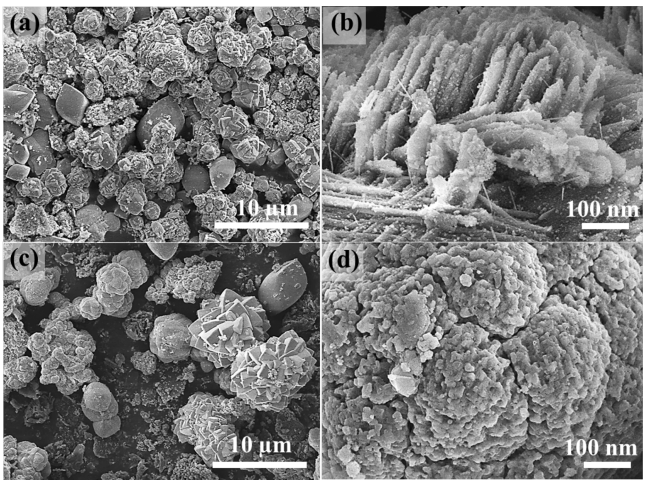

Figure 4. Low- and high-magnification SEM images of (a, b) $MnCO_3$ and (c, d) $MnCO_3$/LIG composite.

conjoint particles and displays a porous 3D flower-like morphology, which comes from the combination of a large network of nanorods,[66] whereas cubic and spherical structures can be seen in the $MnCO_3$/LIG composite, as displayed in Figure 4c,d.[67]

Figure 5 displays the HR-TEM images of the LIG and $MnCO_3$/LIG composite material. Figure 5a highlights LIG's

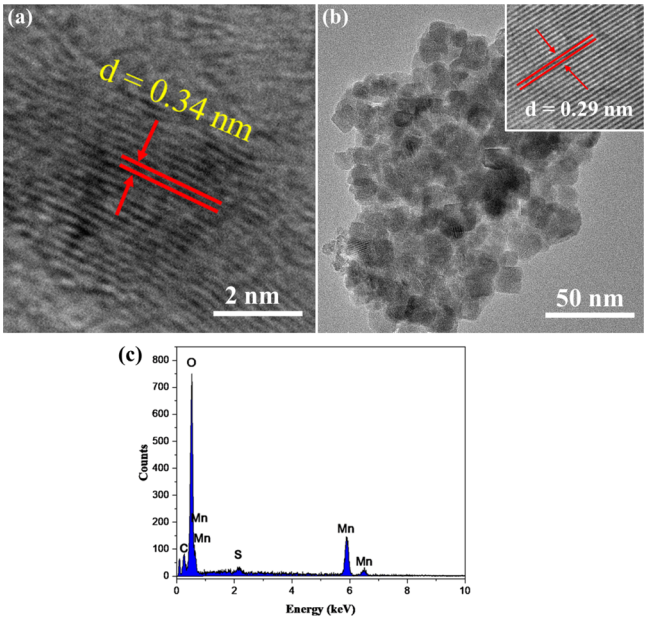

Figure 5. TEM images of scrapped LIG powder and $MnCO_3$/LIG composite; (a) HR-TEM of LIG and (b) $MnCO_3$/LIG; (c) EDS spectrum of $MnCO_3$/LIG.

few-layer structure with an average lattice space of 0.34 nm, which corresponds to the distance between neighboring (002) planes in graphene.[39,61] Figure 5b clearly shows that $MnCO_3$ was stably embedded and uniformly dispersed on LIG. HR-TEM results suggest that $MnCO_3$ has a spherical morphology with a well-defined fringe and interplanar distance (*d*-spacing) of approximately 0.29 nm, which corresponds to the (104) plane of the $MnCO_3$ structure.[66,68] TEM-EDS (Figure 5c) also exhibits C, O, Mn, and S peaks and confirms the formation of the $MnCO_3$/LIG composite.

FTIR spectra of LIG, $MnCO_3$, and $MnCO_3$/LIG are shown in Figure 6. LIG has a broad peak around 3420 cm^{-1},

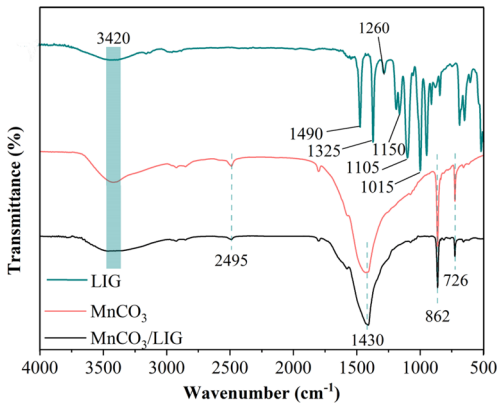

Figure 6. FTIR spectra of LIG, $MnCO_3$, and the $MnCO_3$/LIG composite.

indicating the presence of a hydroxyl group (O−H).[69] The peaks at ∼1490 and 1015 cm^{-1} are resulted from the −C═C stretching and bending vibration, respectively, while peaks at ∼1325 and ∼1150 are associated with the−SO_2 symmetric and asymmetric stretching vibration in PES, respectively.[61] Moreover, additional peaks at 1260 and 1105 cm^{-1} are due to symmetric and asymmetric −C−O−C bands, respectively.[70] The $MnCO_3$ showed peaks at 2495, 1430, 862, and 726 cm^{-1}, corresponding to the framework stretching vibration of $MnCO_3$.[59,71] A broad peak at around 3420 cm^{-1} is attributed to the adsorbed water molecules. All of the peaks were also found at similar wave numbers for the $MnCO_3$/LIG composite, confirming the successful formation of the composite. Taking all of the characterization into account, $MnCO_3$ was fused with the LIG to form the composite structure.

The surface area and porous structure of $MnCO_3$ and $MnCO_3$/LIG were evaluated by nitrogen adsorption−desorption isotherms and the BJH pore size distribution, as shown in Figure 7. More details on the porous structures of $MnCO_3$ and $MnCO_3$/LIG are summarized in Table 1. The $MnCO_3$ and $MnCO_3$/LIG displayed BET surface areas of 11.30 and 8.28 m^2/g, respectively, while the mean pore size and the corresponding pore volume were found to be 9.20 and 11.5 nm and 0.03 and 0.02 cm^3/g, respectively. The nitrogen isotherms for both samples indicate a Type II isotherm, which is a signature of the large pore size distribution within the microporous structure of $MnCO_3$. This relatively large pore size distribution is confirmed by BJH pore size distribution results, as illustrated in Figure 7b,d. The BET result suggests that the prepared samples have a small microporous structure, and most of the porosity is associated with macropores. The BET surface area and pore volume of the $MnCO_3$/LIG composite are lower than those of $MnCO_3$, which can be attributed to the effect of compositing and further processing of $MnCO_3$ that can lead to the less porous structure of $MnCO_3$/LIG composite.

To understand the electrocatalytic behavior of LIG, $MnCO_3$, and $MnCO_3$/LIG composite, tests were carried out using a CV technique at the applied voltage from −0.4 to 0.65 V under

https://doi.org/10.1021/acsomega.3c07642
ACS Omega 2024, 9, 7869−7880

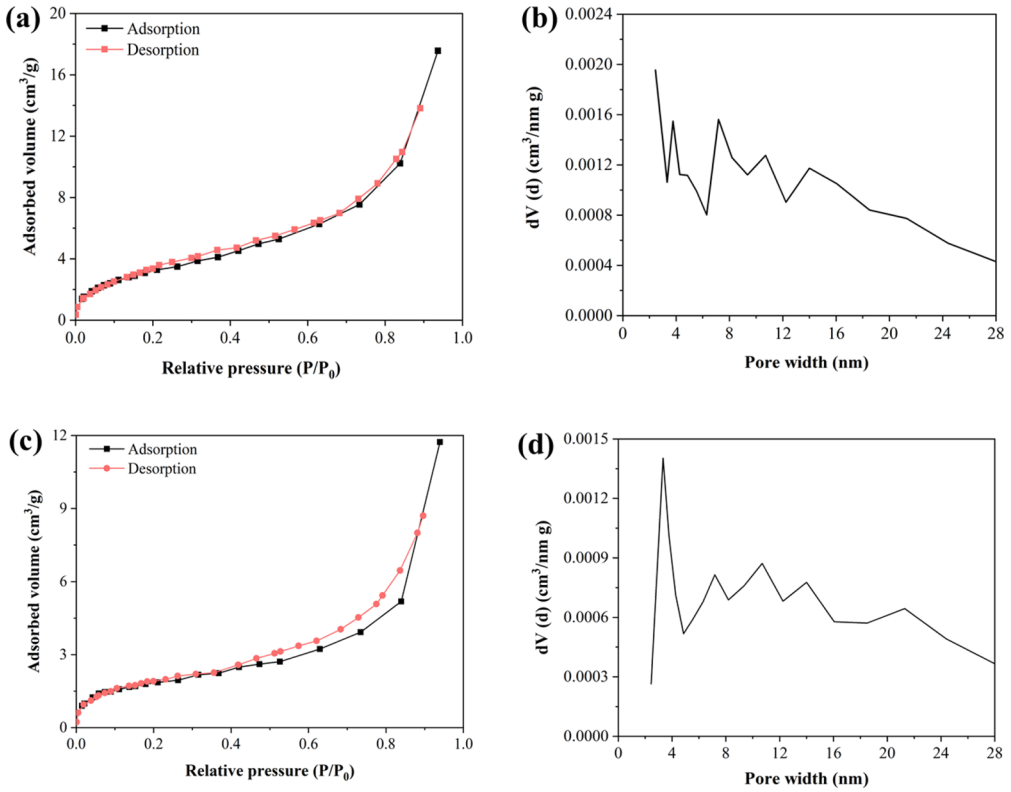

Figure 7. N_2 adsorption−desorption isotherm and pore size distribution of (a, b) $MnCO_3$ and (c, d) $MnCO_3$/LIG composite.

Table 1. BET Surface Area, Average Pore Diameter, and Pore Volume of $MnCO_3$ and $MnCO_3$/LIG Composite

materials	specific surface area (m^2/g)	pore diameter (nm)	pore volume (cm^3/g)
$MnCO_3$	11.80	9.20	0.03
$MnCO_3$/LIG	6.30	11.50	0.02

three-electrode cell configurations in 0.1 M KOH at 50 mV s^{-1}. Figure 8a indicates that the anodic and cathodic peak currents of GC electrodes modified with the $MnCO_3$/LIG composite are much larger than those of electrodes modified with LIG and $MnCO_3$. It can be clearly seen that the $MnCO_3$ and $MnCO_3$/LIG composite electrode exhibits well-defined redox peaks with the anodic peak at around 0.02 and −0.17 V and the cathodic peak at around −0.2 and −0.29 V, which correspond to the electron transfer mechanism that may involve the participation of Mn(II) and Mn(III) or Mn(IV), respectively. The same $MnCO_3$/LIG composite-modified GC electrode was used to detect glucose with concentrations of 3.0 mM. The new peak position can be found at 550 mV (Figure 8b), which is at 3 orders of magnitude larger current than that of the $MnCO_3$-modified GC electrode. It is worth noting that there was no response from the GC electrode that was modified with LIG. Furthermore, the GC electrode modified with $MnCO_3$/LIG composite was evaluated for detecting glucose at different concentrations in the range of 0.5 and 7 mM (Figure 8c). It is observed that the oxidation current increased greatly with the addition of glucose at a scan rate of 50 mV s^{-1}, while the cathodic peak currents are unchanged due to irreversible oxidation process of glucose to glucolactone.[72] For the detection of 5 mM glucose, the peak current of the electrode reached 140 μA, and the peak current for 1 mM glucose was approximately 70 μA. Furthermore, with increasing concentration of glucose, the peak current gets saturated, and the sensitivity decreases.

Figure 9 illustrates the proposed mechanism of glucose oxidation on GC electrodes modified with a $MnCO_3$/LIG composite. The active metal center of Mn* across the electrode undergoes a premonolayer oxidation step and subsequent chemisorption of the glucose molecule by LIG and Mn*. Mn* was adsorbed in the hydrous oxide layer to form a reactive incipient hydrous oxide layer (OH_{ads}) and mediates the glucose oxidation and inhibits reduction reaction. At this state, $Mn[OH]_{ads}$ has low lattice coordination value, and thus, lacks normal lattice stabilization energy, which makes $Mn[OH]_{ads}$ less stable and increases its reactivity. As a result, oxidation of the premonolayer accelerates even at lower potential compared to thermodynamic surface oxidation. Additionally, it is worth noting that the chemisorption of the glucose molecule occurs at $Mn[OH]_{ads}$ sites, and LIG can also facilitate glucose chemisorption on the electrode. The presence of graphene facilitates glucose oxidation at lower potentials.[73−75] Due to good catalytic activity/adsorption of $MnCO_3$ and improved adsorption and conductivity of LIG, the composite sensor displays enhanced sensitive detection to detect glucose. Electrochemical impedance spectroscopy (EIS) can be used to assess the interfacial charge transfer kinetics (R_{ct}) of the bare and different electrode materials, which was obtained by fitting the Nyquist plot. Nyquist plots of the bare, LIG, $MnCO_3$, and $MnCO_3$/LIG-modified GC electrodes evaluated in the presence of the KCl with 5 mM $[Fe(CN)_6]^{3-/4-}$ electrolyte are displayed in Figure S2 in the Supporting Information. Bare and LIG-modified GC electrodes display depressed semicircles in the high-frequency region with R_{ct} values of 810 and 380 Ω, respectively. These results are attributed to the low surface resistance phenomena.

https://doi.org/10.1021/acsomega.3c07642
ACS Omega 2024, 9, 7869−7880

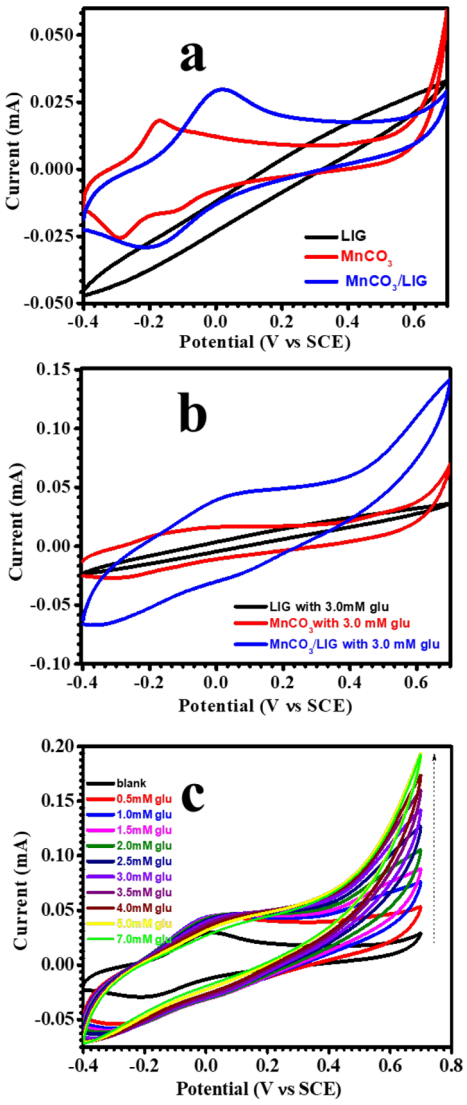

Figure 8. (a) CVs of the different modified GC electrodes without the addition of glucose, (b) CVs of the different modified GC electrodes after the addition of 3 mM glucose concentration with 0.1 M KOH at 50 mV $s^{-1}$and (c) CVs of the $MnCO_3$/LIG-modified GC electrodes in different glucose concentrations with 0.1 M KOH at 50 mV s^{-1}.

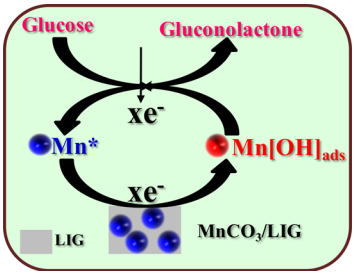

Figure 9. Sensing mechanism of the enzyme-free sensor based on the $MnCO_3$/LIG composite-modified GC electrode.

Further, it is also possible to provide a big semicircle for high charge transfer resistance. $MnCO_3$ exhibits a semicircle with a R_{ct} value of 570 Ω. EIS data can be fit by a proposed equivalent circuit for the $MnCO_3$/LIG-modified GC electrode comprising an ohmic resistance of the solution *Rs*, two charge transfer resistances R_{ct} (R_1 and R_2), as shown in the inset of Figure S2 in the Supporting Information. R_1 represents the electron transfer resistance between the interface of electrode/electrolyte, R_2 represents the charge exchange resistance between active material and electrolyte, and C_{dl} is the capacitance in the electrolyte. R_s of the $MnCO_3$/LIG-modified GC electrode (420 Ω) are smaller than that of the $MnCO_3$ electrode (570 Ω), which shows that the $MnCO_3$/LIG-modified GC electrode facilitates the electron transfer rate owing to the shorter electron transfer path.

$$Mn^* + OH^- \rightarrow Mn[OH]_{ads} \quad (1)$$

$$Mn[OH]_{ads} + xe^- \rightarrow Mn^* \quad (2)$$

$$Glucose \rightarrow Gluconolactone + xe^- \quad (3)$$

$MnCO_3$/LIG was investigated by CV toward the oxidation of glucose in 0.1 M KOH solution with different scan rates (10−100 mV s^{-1}), and results are displayed in Figure 10.

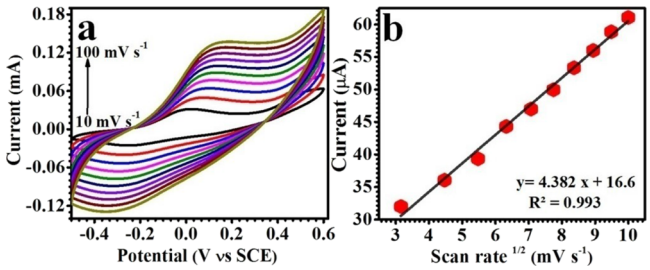

Figure 10. (a) CVs of the $MnCO_3$/LIG-modified GC electrode in 2.5 mM glucose concentrations with 0.1 M KOH at different scan rates and (b) plot of the peak current versus the scan rates.

Before glucose addition, the GC electrode modified with $MnCO_3$/LIG exhibits an anodic peak at 19.1 mV and a cathodic peak at −212 mV (Figure 8a). After glucose addition, the $MnCO_3$/LIG composite-modified GC electrode shows an anodic peak at 96 mV, a cathodic peak at −275 mV, and a glucose oxidation peak at 550 mV. With an increase in the scan rate, both the anodic and cathodic peak currents increase. The anodic peak makes a positive shift in potential, while the cathodic peak shows a slightly negative shift in potential, demonstrating a quasi-reversible electron transfer reaction for the electrochemical reactions. Moreover, the potentials and peak currents of the glucose irreversible process (anodic peak at 550 mV) are dependent on the scan rates. Larger peak-to-peak separations were observed with the increase in scan rates. The anodic peak current values increased linearly with the scan rates (correlation coefficient values of 0.993 for anodic peak) in the scan rate range of 10−100 mV s^{-1} (Figure 10b). The linearity of peak current and scan rate suggests that the kinetics is controlled by the adsorption of glucose. Moreover, to obtain the C_{dl} (double layer capacitance), the voltammetry curves of Figure 10 were used. Assuming that the charging of the electric double layer is solely responsible for the process, a linear behavior is obtained, and the angular coefficient gives the C_{dl}.[76] A linear relationship was obtained when the current was plotted against the scan rate variation, represented in Figure S3, Supporting Information. It showed that good linearity is a good indication that redox transitions contribute little to the chosen potential. Then, the C_{dl} value of the $MnCO_3$/LIG-modified GC electrode was calculated as being 32.4 μF.

The effect of the various applied potentials on glucose oxidation was studied for the $MnCO_3$/LIG-modified GC

https://doi.org/10.1021/acsomega.3c07642
ACS Omega 2024, 9, 7869−7880

electrode in 0.1 M KOH. The applied potentials of 0.5, 0.55, and 0.6 V were chosen. Figure S4 (Supporting Information) demonstrates the amperometric response using a $MnCO_3$/LIG-modified GC electrode after successive addition of 0.1 mM glucose, while the solution was being stirred. Results clearly show that amperometric responses enhance current response at 0.55 V in compared to 0.5 and 0.6 V. So, further experiments were conducted at a fixed potential of 0.55 V for glucose sensor. Figure 11a depicts the amperometric responses

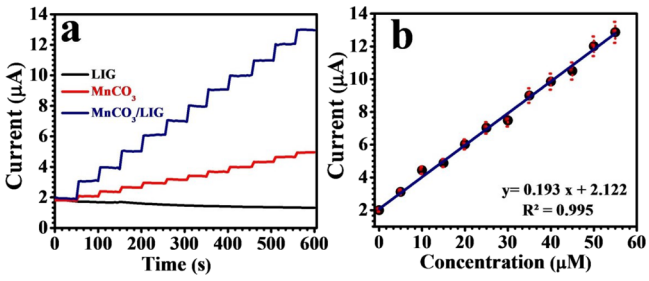

Figure 11. (a) Amperometric responses of the LIG, $MnCO_3$, and $MnCO_3$/LIG-modified GC electrodes after the subsequent addition of 5.0 μM glucose in a 0.1 M KOH solution and (b) relationship between the amperometric responses and the glucose concentrations of the $MnCO_3$/LIG-modified GC electrode.

of various modified GC electrodes to glucose with the subsequent addition of 5.0 μM glucose in a 0.1 M KOH solution for every 50 s. The GC electrode modified with $MnCO_3$/LIG outperformed the other two electrodes in terms of current densities at a fixed potential of 550 mV. After the addition of each dose of glucose into a stirred KOH solution, the oxidation currents of the GC electrode modified with $MnCO_3$/LIG were monitored at a fixed potential of 550 mV, as illustrated in Figure 11a. This curve was used to create the calibration for the GC electrode modified with $MnCO_3$/LIG, as displayed in Figure 11b.

From the amperometric curve for glucose, the linear relationship between the oxidation current and the glucose concentration was obtained for concentrations ranging from 5.0 to 55 μM for $MnCO_3$ and $MnCO_3$/LIG-modified GC electrodes (Figures 11b and S5 in the Supporting Information). The linear regression equation is given by $y = 0.193x + 2.122$, with a correlation coefficient of $R^2 = 0.995$ for the $MnCO_3$-modified GC electrode. The $MnCO_3$/LIG-modified GC electrode exhibits an LOD of 2.2 μM, sensitivity of 2731.2 μA mM^{-1} cm^{-2}, and a limit of quantification (LOQ) of 12.2 μM. The $MnCO_3$/LIG-modified GC electrode outperforms the $MnCO_3$-modified GC electrode (linear regression equation of $y = 0.056x + 1.795$, $R^2 = 0.996$, and LOD of 6.5 μM and sensitivity of 794.2 μA mM^{-1} cm^{-2}). Table 2 summarizes the previously reported enzyme-free glucose sensors with Mn-based composite electrodes. The sensitivity of our $MnCO_3$/LIG-modified GC electrode can be compared against those reported earlier.[45−52,54] Our GC electrode modified with $MnCO_3$/LIG reveals the highest sensitivity, reasonable LOD, and acceptable linear range. This superior performance can be attributed to the synergetic effect of compositing $MnCO_3$ with LIG. The conductive graphene boosts the electrocatalytically active area and promotes electron transfer in glucose oxidation.

During electrochemical glucose sensing, some of the compounds that easily oxidize (e.g., ascorbic acid (AA), dopamine (DA), uric acid (UA)) and always exist with glucose in human blood can interfere with the sensor's glucose detection. Thus, evaluating the anti-interference property of the proposed $MnCO_3$/LIG composite sensor is crucial. The current response of inferences needs to be investigated with a $MnCO_3$/LIG-modified GC electrode for glucose sensor. As shown in Figure 12a, no significant signals can be observed for

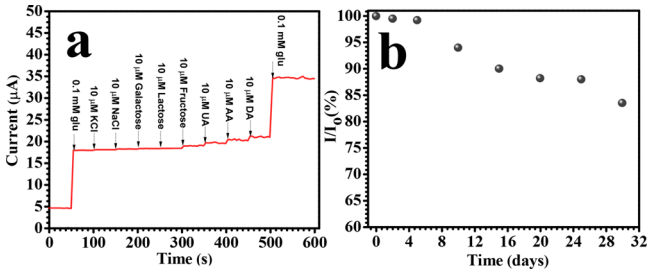

Figure 12. (a) Amperometric response to the sequential addition of 0.1 mM glucose with 10 μM interfering species at 0.55 V and (b) stability of the sensor over 30 days using 0.1 M KOH with 0.5 mM glucose.

interfering species, whereas distinct glucose oxidation currents were obtained. Hence, this result suggests that a small amount of AA, DA, UA, galactose, lactose, fructose, NaCl, and KCl can be tolerated with the $MnCO_3$/LIG-modified GC electrode and confirms the high selectivity for glucose sensing. Figure 12b depicts the stability of the $MnCO_3$/LIG-modified GC electrode evaluated at 0.55 V for the amperometric current responses within 30 days. The electrode was exposed to air and tested for initially 2 days and then every 5 days. The current response of the $MnCO_3$/LIG-modified GC electrode was approximately 90 and 83.5% of its original counterpart after 15 and 30 days, respectively. The reproducibility of the sensor was also tested by measuring the CV response of a glucose solution

Table 2. Comparison of Enzyme-Free Mn-Based Composite Electrodes

electrode composition	sensitivity (μA mM^{-1} cm^{-2})	linear range (mM)	LOD (μM)	ref.
Mn_3O_4/3DGF	360	0.01−8	10	45
Mn_3O_4/N-GR	101.1	0.0025−0.5295	1	46
Nafion/Co/MnO@HC/GCE	233.8	Up to 6.9	1.31	47
MnO_2/MWNTs	33.19	0.01−28	3.3	48
Cu/MnO_2/MWCNTs	1302	0.00064−2.2	1.7	49
Nafion/Mn−Ni-oxide/GCE	82.44	0.1−1	0.2	50
$NiMn_2O_4$NSs@rGO	2615.2	0.001−3.5		51
α-MnO_2/Co_3O_4	127	0.06−7	0.03	52
$MnCO_3$/Ni foam	1254.4	0.001−0.5	1	54
$MnCO_3$/LIG/GCE	2731.2	0.005−0.055	2.2	this work

https://doi.org/10.1021/acsomega.3c07642
ACS Omega 2024, 9, 7869−7880

for 10 consecutive tests. Results displayed an excellent reproducibility with a relative standard deviation as low as 3.38% and mean value of 20.53 μA (Figure S6, Supporting Information). Reasonable stability and reproducibility of the $MnCO_3$/LIG-modified GC electrode are attributed to its unparalleled chemically stable $MnCO_3$ phase and electrochemically stable LIG under this condition.

The application of the $MnCO_3$/LIG-modified GC electrode was studied for glucose detection in blood serum samples, which were collected from local hospitals. The serum was processed by diluting with distilled water and centrifuged with at 5000 rpm for 10 min. The supernatant liquid was withdrawn for further evaluation. Various concentrations of the sample were added into the 0.1 M KOH, and the current response was recorded. Table 3 summarizes the recovery results of the glucose sensor in serum samples. To further confirm the glucose detection, the known concentration of glucose was added to the 0.1 M KOH. The $MnCO_3$/LIG-modified GC electrode exhibited good recovery (98.7−99.3%) of glucose in blood serum samples, which confirmed its capability toward practical applications.

Table 3. $MnCO_3$/LIG-Modified GC Electrode-Based Glucose Sensor in Blood Serum Samples

sample	added (μM)	found (μM)	recovery (%)
blood serum		6.55	
	15	14.81	98.73
	30	29.75	99.16
	50	49.75	99.50

CONCLUSIONS

In this work, we successfully prepared the $MnCO_3$/LIG composite and used it as an electrode for glucose detection. The LIG was fabricated in a single step on a PES substrate by using a CO_2 infrared laser. Through a simple hydrothermal synthesis method, we obtained $MnCO_3$-decorated LIG. Then, the $MnCO_3$/LIG composite was immobilized onto a GCE surface. Then, the composite structure was successfully characterized by employing different techniques. Following this, we successfully demonstrated the suitability of the $MnCO_3$/LIG-modified GC electrode for glucose detection by using electroanalytical techniques. The possible mechanism of $MnCO_3$/LIG for glucose detection was found to be good catalytic activity and chemisorption of $MnCO_3$ and good conductivity with the improved chemisorption nature of LIG of the glucose molecule. Overall, this electrode exhibited significantly improved performance compared to the previously Mn-based composite. The superior performance is attributed to the conductive nature and electrocatalytic active areas of LIG in the $MnCO_3$/LIG composite, which facilitate direct electron transfer, resulting in enhanced detection of glucose. Benefiting from its unique properties, the composite showed an excellent sensitivity of 2731.2 $\mu A\ mM^{-1}\ cm^{-2}$ with a detection limit of 2.2 μM. This work provides new insight into LIG materials to design efficient electrodes for sensing applications. It demonstrates better sensitivity, wide linear range, and good selectivity for a glucose sensor, which may provide new directions for exploiting advanced materials for other electrochemical biosensors and energy storage devices.

ASSOCIATED CONTENT

Supporting Information

The Supporting Information is available free of charge at https://pubs.acs.org/doi/10.1021/acsomega.3c07642.

XPS survey of the MnCO3/LIG composite; electrochemical performance evaluation, including EIS of different modified GC electrodes, variation of current in double layer as a function of scan rate, and GC electrode sensor performance at different potentials; and reproducibility of the $MnCO_3$/LIG glucose sensor (PDF)

AUTHOR INFORMATION

Corresponding Author

Mahdi Malmali − *Department of Chemical Engineering, Texas Tech University, Lubbock, Texas 79409, United States;* orcid.org/0000-0001-5190-1261; Phone: (806) 834-8706; Email: mahdi.malmali@ttu.edu; Fax: (806) 742-3552

Authors

Amit K. Thakur − *Department of Chemical Engineering, Texas Tech University, Lubbock, Texas 79409, United States;* Present Address: Mojave Energy System Inc., Palo Alto, California 94304, United States (A.K.T.); orcid.org/0000-0003-1409-6202

Prakash Sengodu − *Department of Industrial Chemistry, School of Chemical Sciences, Alagappa University, Karaikudi, Tamil Nadu 630003, India*

Arvind H. Jadhav − *Centre for Nano and Material Science (CNMS), Jain University, Bangalore 562112, India;* orcid.org/0000-0002-9128-1981

Complete contact information is available at: https://pubs.acs.org/10.1021/acsomega.3c07642

Author Contributions

‖A.K.T. and P.S. contributed equally to this work.

Notes

The authors declare no competing financial interest.

ACKNOWLEDGMENTS

A.K.T. and M.M. acknowledge partial financial support from the RAPID Manufacturing Institute, a public−private partnership between the US Department of Energy and the American Institute of Chemical Engineers (AIChE). This material is based upon work supported by the Department of Energy's Office of Energy Efficiency & Renewable Energy's Advanced Manufacturing Office under Award Number DE-EE0007888, Subtask 8.8.

REFERENCES

(1) WHO Global Report, *Global Report on Diabetes, ISBN 978*; 2016, 11.

(2) Wang, J. Electrochemical Glucose Biosensors. *Chem. Rev.* **2008**, *108*, 814−825, DOI: 10.1021/cr068123a.

(3) Jia, W. Z.; Wang, K.; Zhu, Z. J.; Song, H. T.; Xia, X. H. One-step immobilization of glucose oxidase in a silica matrix on a Pt electrode by an electrochemically induced sol-gel process. *Langmuir.* **2007**, *23*, 11896−11900.

(4) Liu, W.; Wu, H.; Li, B.; Dong, C.; Choi, M. M. F.; Shuang, S. Immobilization of platinum nanoparticles and glucose oxidase on eggshell membrane for glucose detection. *Analytical Methods.* **2013**, *5*, 5154−5160.

(5) Lipińska, W.; Siuzdak, K.; Karczewski, J.; Dołęga, A.; Grochowska, K. Electrochemical glucose sensor based on the glucose oxidase entrapped in chitosan immobilized onto laser-processed Au-Ti electrode. *Sensors and Actuators B: Chemical.* **2021**, *330*, No. 129409.
(6) Chen, T.; Liu, D.; Lu, W.; Wang, K.; Du, G.; Asiri, A. M.; Sun, X. Three-dimensional Ni_2P Nanoarray: An efficient catalyst electrode for sensitive and selective nonenzymatic glucose sensing with high specificity. *Anal. Chem.* **2016**, *88*, 7885−7889.
(7) Wang, Z.; Cao, X.; Liu, D.; Hao, S.; Kong, R.; Du, G.; Asiri, A. M.; Sun, X. Copper-Nitride Nanowires Array: An efficient dual-functional catalyst electrode for sensitive and selective non-enzymatic glucose and hydrogen peroxide sensing. *Chem.—Eur. J.* **2017**, *23*, 4986−4989.
(8) Wei, M.; Qiao, Y.; Zhao, H.; Liang, J.; Li, T.; Luo, Y.; Lu, S.; Shi, X.; Lu, W.; Sun, X. Electrochemical non-enzymatic glucose sensors: recent progress and perspectives. *Chemical Communications.* **2020**, *56*, 14553−14569.
(9) Qiao, Y.; Liu, Q.; Lu, S.; Chen, G.; Gao, S.; Lu, W.; Sun, X. High-performance non-enzymatic glucose detection: using a conductive Ni-MOF as an electrocatalyst. *J. Mater. Chem. B* **2020**, *8*, 5411−5415.
(10) Xie, F.; Cao, X.; Qu, F.; Asiri, A. M.; Sun, X. Cobalt nitride nanowire array as an efficient electrochemical sensor for glucose and H_2O_2 detection, Sensors and Actuators, B. *Chemical.* **2018**, *255*, 1254−1261.
(11) Marini, S.; Ben Mansour, N.; Hjiri, M.; Dhahri, R.; El Mir, L.; Espro, C.; Bonavita, A.; Galvagno, S.; Neri, G.; Leonardi, S. G. Non-enzymatic Glucose Sensor Based on Nickel/Carbon Composite. *Electroanalysis.* **2018**, *30*, 727−733.
(12) Şavk, A.; Aydın, H.; Cellat, K.; Şen, F., A novel high performance non-enzymatic electrochemical glucose biosensor based on activated carbon-supported Pt-Ni nanocomposite, *J. Mol. Liq. 300* (**2020**). DOI: 112355.
(13) Mei, H.; Wu, W.; Yu, B.; Li, Y.; Wu, H.; Wang, S.; Xia, Q. Non-enzymatic sensing of glucose at neutral pH values using a glassy carbon electrode modified with carbon supported Co@Pt core-shell nanoparticles. *Microchimica Acta.* **2015**, *182*, 1869−1875.
(14) Yang, J.; Liang, X.; Cui, L.; Liu, H.; Xie, J.; Liu, W. A novel non-enzymatic glucose sensor based on Pt3Ru1 alloy nanoparticles with high density of surface defects. *Biosensors and Bioelectronics.* **2016**, *80*, 171−174.
(15) Bai, Y.; Sun, Y.; Sun, C. Pt-Pb nanowire array electrode for enzyme-free glucose detection. *Biosensors and Bioelectronics.* **2008**, *24*, 579−585.
(16) Ye, J. S.; Wen, Y.; De Zhang, W.; Gan, L. M.; Xu, G. Q.; Sheu, F. S. Nonenzymatic glucose detection using multi-walled carbon nanotube electrodes. *Electrochem. Commun.* **2004**, *6*, 66−70.
(17) Wang, J.; Sun, X.; Cai, X.; Lei, Y.; Song, L.; Xie, S. S. Nonenzymatic glucose sensor using freestanding single-wall carbon nanotube films. *Electrochem. Solid-State Lett.* **2007**, *10*, 58−60.
(18) Zhang, C.; Zhang, Z.; Yang, Q.; Chen, W. Graphene-based Electrochemical Glucose Sensors: Fabrication and Sensing Properties. *Electroanalysis.* **2018**, *30*, 2504−2524.
(19) Alwarappan, S.; Liu, C.; Kumar, A.; Li, C. Z. Enzyme-doped graphene nanosheets for enhanced glucose biosensing. *J. Phys. Chem. C* **2010**, *114*, 12920−12924.
(20) Kang, X.; Wang, J.; Wu, H.; Aksay, I. A.; Liu, J.; Lin, Y. Glucose Oxidase-graphene-chitosan modified electrode for direct electrochemistry and glucose sensing. *Biosensors and Bioelectronics.* **2009**, *25*, 901−905.
(21) Shao, Y.; Wang, J.; Wu, H.; Liu, J.; Aksay, I. A.; Lin, Y. Graphene based electrochemical sensors and biosensors: A review. *Electroanalysis.* **2010**, *22*, 1027−1036.
(22) Wang, Y.; Shao, Y.; Matson, D. W.; Li, J.; Lin, Y. Nitrogen-Doped Graphene and Its Biosensing. *ACS Nano* **2010**, *4*, 1790−1798.
(23) Kong, F. Y.; Li, X. R.; Zhao, W. W.; Xu, J. J.; Chen, H. Y. Graphene oxide-thionine-Au nanostructure composites: Preparation and applications in non-enzymatic glucose sensing. *Electrochem. Commun.* **2012**, *14*, 59−62.
(24) Apelgren, P.; Amoroso, M.; Säljö, K.; Montelius, M.; Lindahl, A.; StridhOrrhult, L.; Gatenholm, P.; Kölby, L.; Arulkumar, S.; Parthiban, S.; Goswami, A.; Varma, R. S.; Naushad, Mu; Gawande, M. B.; Lipskas, J.; Deep, K.; Yao, W.; Grogan, S. P.; Dorthé, E. W.; Glembotski, N. E.; Gaul, F.; D'Lima, D. D.; Beketov, E. E.; Isaeva, E. V.; Yakovleva, N. D.; Demyashkin, G. A.; Arguchinskaya, N. V.; Kisel, A. A.; Lagoda, T. S.; Malakhov, E. P.; Kharlov, V. I.; Osidak, E. O.; Domogatsky, S. P.; Ivanov, S. A.; Shegay, P. V.; Kaprin, A. D.; Sun, Y.; Wu, Q.; Zhang, Y.; Dai, K.; Wei, Y.; Dhawan, A.; Kennedy, P. M.; Rizk, E. B.; Ozbolat, I. T.; Ma, K.; Zhao, T.; Yang, L.; Wang, P.; Jin, J.; Teng, H.; Xia, D.; Zhu, L.; Li, L.; Jiang, Q.; Wang, X.; Fiscale, C.; In, R.; E-mail, I.; Personal, S.; Credit, S.; Trattamento, T. D. E. L.; Tel, T.; Della, R.; Dei, P.; Adempiere, D. I.; Un, A. D.; Di, O.; Salvatore, D. A. Gold − graphene oxide nanocomposites for enzyme-less glucose monitoring. *Mater. Today: Proc.* **2019**, *27*, No. 065002.
(25) Chang, G.; Shu, H.; Huang, Q.; Oyama, M.; Ji, K.; Liu, X.; He, Y. Synthesis of highly dispersed Pt nanoclusters anchored graphene composites and their application for non-enzymatic glucose sensing. *Electrochim. Acta* **2015**, *157*, 149−157.
(26) Xiao, F.; Li, Y.; Gao, H.; Ge, S.; Duan, H. Growth of coral-like PtAu-MnO2 binary nanocomposites on free-standing graphene paper for flexible nonenzymatic glucose sensors. *Biosensors and Bioelectronics.* **2013**, *41*, 417−423.
(27) Yang, S.; Li, G.; Wang, G.; Zhao, J.; Gao, X.; Qu, L. Synthesis of Mn3O4 nanoparticles/nitrogen-doped graphene hybrid composite for nonenzymatic glucose sensor, Sensors and Actuators, B. *Chemical.* **2015**, *221*, 172−178.
(28) Yang, S.; Liu, L.; Wang, G.; Li, G.; Deng, D.; Qu, L. One-pot synthesis of Mn3O4 nanoparticles decorated with nitrogen-doped reduced graphene oxide for sensitive nonenzymatic glucose sensing. *J. Electroanal. Chem.* **2015**, *755*, 15−21.
(29) Ruiyi, L.; Juanjuan, Z.; Zhouping, W.; Zaijun, L.; Junkang, L.; Zhiguo, G.; Guangli, W. Novel graphene-gold nanohybrid with excellent electrocatalytic performance for the electrochemical detection of glucose, Sensors and Actuators, B. *Chemical.* **2015**, *208*, 421−428.
(30) Lin, J.; Peng, Z.; Liu, Y.; Ruiz-Zepeda, F.; Ye, R.; Samuel, E. L. G. G.; Yacaman, M. J.; Yakobson, B. I.; Tour, J. M. Laser-induced porous graphene films from commercial polymers, Nature. *Communications.* **2014**, *5*, 5−12.
(31) Singh, S. P.; Li, Y.; Zhang, J.; Tour, J. M.; Arnusch, C. J.; Singh, S. P.; Li, Y.; Zhang, J.; Tour, J. M.; Arnusch, C. J. Sulfur-doped laser-induced porous graphene derived from polysulfone-class polymers and membranes. *ACS Nano* **2018**, *12*, 289−297.
(32) Stanford, M. G.; Zhang, C.; Fowlkes, J. D.; Hoffman, A.; Ivanov, I. N.; Rack, P. D.; Tour, J. M. High-Resolution Laser-Induced Graphene. Flexible Electronics beyond the Visible Limit. *ACS Appl. Mater. Interfaces* **2020**, *12*, 10902−10907.
(33) Chyan, Y.; Ye, R.; Li, Y.; Singh, S. P.; Arnusch, C. J.; Tour, J. M. Laser-Induced Graphene by Multiple Lasing: Toward Electronics on Cloth, Paper, and Food. *ACS Nano* **2018**, *12*, 2176−2183.
(34) Thakur, A. K.; Singh, S. P.; Gupta, A.; Arnusch, C. J. Laser-Induced Graphene − PVA Composites as Robust Electrically Conductive Water Treatment Membranes. *ACS Appl. Mater. Interfaces* **2019**, *11*, 10914−10921.
(35) Kulyk, B.; Silva, B.; Carvalho, A.; Silvestre, S.; Fernandes, A.; Martins, R.; Fortunato, E.; Costa, F. Laser-Induced Graphene from Paper for Mechanical Sensing. *ACS Applied Materials & Interfaces.* **2021**, *13*, 10210.
(36) Vivaldi, F. M.; Dallinger, A.; Bonini, A.; Poma, N.; Sembranti, L.; Biagini, D.; Salvo, P.; Greco, F.; Di Francesco, F. Three-Dimensional (3D) Laser-Induced Graphene: Structure, Properties, and Application to Chemical Sensing. *ACS Appl. Mater. Interfaces* **2021**, *13*, 30245−30260.
(37) Mahbub, H.; Saed, M. A.; Malmali, M. Pattern-Dependent Radio Frequency Heating of Laser-Induced Graphene Flexible Heaters. *ACS Appl. Mater. Interfaces* **2023**, *15* (14), 18074−18086.

https://doi.org/10.1021/acsomega.3c07642
ACS Omega 2024, 9, 7869−7880

(38) Thamaraiselvan, C.; Thakur, A. K.; Gupta, A.; Arnusch, C. J. Electrochemical Removal of Organic and Inorganic Pollutants Using Robust Laser-Induced Graphene Membranes. *ACS Applied Materials and Interfaces.* **2021**, *13*, 1452−1462.
(39) Thakur, A. K.; Lin, B.; Nowrin, F. H.; Malmali, M. Comparing Structure and Sorption Characteristics of Laser-Induced Graphene (LIG) from Various Polymeric Substrates. *ACS Environmental Science and Technology Water.* **2022**, *2*, 75−87.
(40) Rathinam, K.; Singh, S. P.; Li, Y.; Kasher, R.; Tour, J. M.; Arnusch, C. J. Polyimide derived laser-induced graphene as adsorbent for cationic and anionic dyes. *Carbon.* **2017**, *124*, 515−524.
(41) Zhu, J.; Liu, S.; Hu, Z.; Zhang, X.; Yi, N.; Tang, K.; Dexheimer, M. G.; Lian, X.; Wang, Q.; Yang, J.; Gray, J.; Cheng, H. Laser-induced graphene non-enzymatic glucose sensors for on-body measurements. *Biosensors and Bioelectronics.* **2021**, *193*, No. 113606.
(42) Settu, K.; Chiu, P.T.; Huang, Y.M., Laser-induced graphene-based enzymatic biosensor for glucose detection, *Polymers. 13* (**2021**). DOI: 2795.
(43) Zhang, Y.; Li, N.; Xiang, Y.; Wang, D.; Zhang, P.; Wang, Y.; Lu, S.; Xu, R.; Zhao, J. A flexible non-enzymatic glucose sensor based on copper nanoparticles anchored on laser-induced graphene. *Carbon.* **2020**, *156*, 506−513.
(44) Zhao, J.; Zheng, C.; Gao, J.; Gui, J.; Deng, L.; Wang, Y.; Xu, R. Co_3O_4 nanoparticles embedded in laser-induced graphene for a flexible and highly sensitive enzyme-free glucose biosensor. *Sensors and Actuators B: Chemical.* **2021**, *347*, No. 130653.
(45) Si, P.; Dong, X.-C.; Chen, P.; Kim, D.-H. A hierarchically structured composite of Mn_3O_4/3D graphene foam for flexible nonenzymatic biosensors. *J. Mater. Chem. B* **2013**, *1*, 110−115.
(46) Yang, S.; Li, G.; Wang, G.; Zhao, J.; Gao, X.; Qu, L. Synthesis of Mn3O4 nanoparticles/nitrogen-doped graphene hybrid composite for nonenzymatic glucose sensor. *Sens. Actuators, B* **2015**, *221*, 172−178.
(47) Zhang, Y.; Huang, Y.; Gao, P.; Yin, W.; Yin, M.; Pu, H.; Sun, Q.; Liang, X.; Fa, H. B. Bimetal-organic frameworks MnCo-MOF-74 derived Co/MnO@HC for the construction of a novel enzyme-free glucose sensor. *Microchemical Journal* **2022**, *175*, No. 107097.
(48) Chen, J.; Zhang, W. D.; Ye, J. S. Nonenzymatic electrochemical glucose sensor based on MnO_2/MWNTs nanocomposite. *Electrochem. Commun.* **2008**, *10*, 1268−1271.
(49) Wang, Y.; Zhang, S.; Bai, W.; Zheng, J. Layer-by-layer assembly of copper nanoparticles and manganese dioxide-multiwalled carbon nanotubes film: A new nonenzymatic electrochemical sensor for glucose. *Talanta* **2016**, *149*, 211−216.
(50) Wang, D.; Cai, D.; Wang, C.; Liu, B.; Wang, L.; Liu, Y.; Li, H.; Wang, Y.; Li, Q.; Wang, T. Muti-component nanocomposite of nickel and manganese oxides with enhanced stability and catalytic performance for non-enzymatic glucose sensors. *Nanotechnology* **2016**, *27*, No. 255501.
(51) Dong, M.; Hu, H.; Ding, S.; Wan g, C.; Li, L. Fabrication of $NiMn_2O_4$ nanosheets on reduced graphene oxide for non-enzymatic detection of glucose. *Mater. Technol.* **2020**, *36*, 203−211.
(52) Sinha, L.; Pakhira, S.; Bhojane, P.; Mali, S.; Hong, C. K.; Shirage, P. M. Hybridization of Co_3O_4 and α-MnO_2 nanostructures for high-performance nonenzymatic glucose sensing. *ACS Sustainable Chemistry & Engineering.* **2018**, *6*, 13248−13261.
(53) Zhao, S.; Feng, F.; Yu, F.; Shen, Q. Flower-to-petal structural conversion and enhanced interfacial storage capability of hydrothermally crystallized $MnCO_3$ via the in situ mixing of graphene oxide. *Journal of Materials Chemistry A* **2015**, *3*, 24095−24102.
(54) Dong, C.; Tao, Y.; Chang, Q.; Liu, Q.; Guan, H.; Chen, G.; Wang, Y. Direct growth of $MnCO_3$ on Ni foil for a highly sensitive nonenzymatic glucose sensor. *J. Alloys Compd.* **2018**, *762*, 216−221.
(55) Zhao, C.; Shao, C.; Li, M.; Jiao, K. Flow-injection analysis of glucose without enzyme based on electrocatalytic oxidation of glucose at a nickel electrode. *Talanta.* **2007**, *71*, 1769−1773.
(56) Fleischmann, M.; Korinek, K.; Pletcher, D. The oxidation of organic compounds at a nickel anode in alkaline solution. *J. Electroanal. Chem.* **1971**, *31*, 39−49.
(57) Zhu, J.; Cho, M.; Li, Y.; Cho, I.; Suh, J. H.; Suh, D.; Orbe, D. D.; Jeong, Y.; Ren, T.-L.; Park, I. Biomimetic turbinate-like artificial nose for hydrogen detection based on 3D porous laser-induced graphene. *ACS Appl. Mater. Interfaces* **2019**, *11* (27), 24386−24394.
(58) Xia, Q. X.; San Hui, K.; Hui, K. N.; Kim, S. D.; Lim, J. H.; Choi, S. Y.; Zhang, L. J.; Mane, R. S.; Yun, J. M.; Kim, K. H. Facile synthesis of manganese carbonate quantum dots/Ni$(HCO_3)^{2}$-$MnCO_3$ composites as advanced cathode materials for high energy density asymmetric supercapacitors. *Journal of Materials Chemistry A* **2015**, *3*, 22102−22117.
(59) Zhou, L.; Kong, X.; Gao, M.; Lian, F.; Li, B.; Zhou, Z.; Cao, H. Hydrothermal fabrication of MnCO3@rGO composite as an anode material for high-performance lithium ion batteries. *Inorganic Chemistry.* **2014**, *53*, 9228−9234.
(60) Luong, D. X.; Yang, K.; Yoon, J.; Singh, S. P.; Wang, T.; Arnusch, C. J.; Tour, J. M. Laser-Induced Graphene Composites as Multifunctional Surfaces. *ACS Nano* **2019**, No. 8b09626.
(61) Malmali, M.; Thakur, A.K.; Mahbub, H.; Nowrin, F.H. Highly robust laser-induced graphene (LIG) ultrafiltration membrane with a stable microporous structure. *ACS Appl. Mater. Interfaces* **2022**, *14*, 46884−46895, DOI: 10.1021/acsami.2c09563.
(62) Thakur, A. K.; Singh, S. P.; Thamaraiselvan, C.; Nunes, M.; Arnusch, C. J. Graphene Oxide on Laser-Induced Graphene Fi Lters for Antifouling, Electrically Conductive Ultra Fi Ltration Membranes. *J. Membr. Sci.* **2019**, *591*, No. 117322.
(63) Liu, H.; Xie, Y.; Liu, J.; Moon, K. Sik; Lu, L.; Lin, Z.; Yuan, W.; Shen, C.; Zang, X.; Lin, L.; Tang, Y.; Wong, C. P. Laser-Induced and KOH-Activated 3D Graphene: A Flexible Activated Electrode Fabricated via Direct Laser Writing for in-Plane Micro-Supercapacitors. *Chem. Eng. J.* **2020**, *393*, No. 124672.
(64) Karuppaiah, M.; Akilan, R.; Sakthivel, P.; Asaithambi, S.; Shankar, R.; Yuvakkumar, R.; Hayakawa, Y.; Ravi, G. Synthesis of self-assembled micro/nano structured manganese carbonate for high performance, long lifespan asymmetric supercapacitors and investigation of atomic-level intercalation properties of OH^- ions via first principle calculation. *Journal of Energy Storage.* **2020**, *27*, No. 101138.
(65) Ge, L.; Hong, Q.; Li, H.; Liu, C.; Li, F. Direct-Laser-Writing of Metal Sulfide-Graphene Nanocomposite Photoelectrode toward Sensitive Photoelectrochemical Sensing. *Advanced Functional Materials.* **2019**, *29*, 1−10.
(66) Prasad, D.; Patil, K. N.; Dateer, R. B.; Kim, H.; Nagaraja, B. M.; Jadhav, A. H. Basicity controlled MgCo2O4 nanostructures as catalyst for viable fixation of CO2 into epoxides at atmospheric pressure. *Chemical Engineering Journal.* **2021**, *405*, No. 126907.
(67) Jia, Y.; Yang, L.; Feng, R.; Ma, H.; Fan, D.; Yan, T.; Feng, R.; Du, B.; Wei, Q. MnCO 3 as a new electrochemiluminescence emitter for ultrasensitive bioanalysis of β-Amyloid 1−42 oligomers based on site-directed immobilization of antibody. *ACS Applied Materials and Interfaces.* **2019**, *11*, 7157−7163.
(68) Xiao, L.; Wang, S.; Wang, Y.; Meng, W.; Deng, B.; Qu, D.; Xie, Z.-Z.; Liu, J. High-capacity and self-stabilized manganese carbonate microspheres as anode material for lithium-ion batteries. *ACS Appl. Mater. Interfaces* **2016**, *8*, 25369−25378.
(69) Sindhu, B.; Kothuru, A.; Sahatiya, P.; Goel, S.; Nandi, S. Laser-induced graphene printed wearable flexible antenna-based strain sensor for wireless human motion monitoring. *EEE Transactions on Electron Devices* **2021**, *68*, 3189−3194.
(70) Zhu, S.; Shi, M.; Zhao, S.; Wang, Z.; Wang, J.; Wang, S. Preparation and Characterization of a Polyethersulfone/Polyaniline Nanocomposite Membrane for Ultrafiltration and as a Substrate for a Gas Separation Membrane. *RSC Adv.* **2015**, *5* (34), 27211−27223.
(71) Cheng, Y.; Zhang, S.; Kang, N.; Huang, J.; Lv, X.; Wen, K.; Ye, S.; Chen, Z.; Zhou, X.; Ren, L. Polydopamine-coated manganese carbonate nanoparticles for amplified magnetic resonance imaging-guided photothermal therapy. *ACS Appl. Mater. Interfaces* **2017**, *9*, 19296−19306, DOI: 10.1021/acsami.7b03087.
(72) Yu, S.; Peng, X.; Cao, G.; Zhou, M.; Qiao, L.; Yao, J.; He, H. Ni nanoparticles decorated titania nanotube arrays as efficient non-enzymatic glucose sensor. *Electrochim. Acta* **2012**, *76*, 512−517.

https://doi.org/10.1021/acsomega.3c07642
ACS Omega 2024, 9, 7869−7880

(73) Vassilyev, Y. B.; Khazova, O. A.; Nikolaeva, N. N. Kinetics and mechanism of glucose electrooxidation on different electrode-catalysts. Part I. Adsorption and oxidation on platinum. *J. Electroanal. Chem.* **1985**, *196*, 105−125.
(74) Beden, B.; Largeaud, F.; Kokoh, K. B.; Lamy, C. Fourier transform infrared reflectance spectroscopic investigation of the electrocatalytic oxidation of D-glucose: Identification of reactive intermediates and reaction products. *Electrochim. Acta* **1996**, *41*, 701−709.
(75) Vassilyev, Y. B.; Khazova, O. A.; Nikolaeva, N. N. Kinetics and mechanism of glucose electrooxidation on different electrode-catalysts. Part II. Effect of the nature of the electrode and the electrooxidation mechanism. *J. Electroanal. Chem.* **1985**, *196*, 127−144.
(76) De Souza, F. A.; Da Rocha, R. C. F.; Vieira, N. S.; Cestarolli, D. T.; Guerra, E. M. Electrochemical studies of V_2O_5/GO_x for glucose detection. *Bull. Mater. Sci.* **2020**, *43*, 283.

https://doi.org/10.1021/acsomega.3c07642
ACS Omega 2024, 9, 7869−7880